Impact of nonlinear growth of the large-scale structure on CMB B-mode delensing

Toshiya Namikawa and Ryuichi Takahashi

Impact of nonlinear growth of the large-scale structure on CMB B-mode delensing

Toshiya Namikawa[1] and Ryuichi Takahashi[2]

[1]*Leung Center for Cosmology and Particle Astrophysics,*
National Taiwan University, Taipei, 10617, Taiwan
[2]*Faculty of Science and Technology, Hirosaki University,*
3 Bunkyo-cho, Hirosaki, Aomori 036-8561, Japan

We study the impact of the nonlinear growth of the large-scale structure (LSS) on the removal of the gravitational lensing effect (delensing) in cosmic microwave background (CMB) B modes. The importance of the nonlinear growth of the LSS in the gravitational lensing analysis of CMB has been recently recognized by several works, while its impact on delensing is not yet explored. The delensing using mass-tracers such as galaxies and cosmic infrared background (CIB) could be also affected by the nonlinear growth. We find that the nonlinear growth of the LSS leads to $\sim 0.3\%$ corrections to B-mode spectrum after delensing with a high-z mass tracer ($z_m \sim 2$) at $\ell = 1000$-2000. The off-diagonal correlation coefficients of the lensing B-mode template spectrum become significant for delensing with low-z tracers ($z_m \lesssim 0.5$), but are negligible with high-z tracers (such as CIB). On the other hand, the power spectrum covariance of the delensed B mode is not significantly affected by the nonlinear growth of the LSS, and the delensing efficiency is not significantly changed even if we use low-z tracers. The CMB B-mode internal delensing is also not significantly affected by the nonlinear growth.

I. INTRODUCTION

The gravitational waves generated at the inflationary era induce the curl pattern in the cosmic microwave background (CMB) polarization map, the so-called B mode (see e.g. [1] and references therein). The detection of the large-scale B mode by the inflationary gravitational waves (IGWs) will open a new window to the early universe. The CMB experiments in the near future such as BICEP Array [2] and Simons Observatory [3] will be able to precisely measure the B mode, and significantly improve the sensitivity to the IGWs.

The current upper bound on the amplitude of the IGWs (the so-called tensor-to-scalar ratio) is $r < 0.07$ (95% C.L.) [4]. Since the lensing effect converts part of E mode to B mode, the removal of the lensing contamination (delensing) increases the signal-to-noise of the tiny IGW signals (e.g., [5–10]). The measured CMB lensing potential and/or tracers of the underlying matter distribution such as galaxies and cosmic infrared background (CIB) can be used to estimate the E-to-B leakage by lensing, or to perform the inverse remapping of the lensed CMB map to reduce the lensing effect in the observed CMB map.

So far multiple works have discussed the feasibility of the delensing of CMB anisotropies in future experiments by the reconstruction of lensing potential internally (e.g., [11–16]) and/or by employing external data such as CIB and radio galaxies (e.g., [17–19]). Several works have already demonstrated the delensing using existing data [20–23]. The impact of the nonlinear growth of the large-scale structure (LSS) is, however, not yet explored. Compared to the low-z lensing, the lensing effect on CMB mostly comes from the gravitational potential at high redshifts, and is not significantly affected by the nonlinear growth of the underlying density fluctuations. However, some recent studies show that the nonlinear growth significantly affects the measurement of the lensing power spectrum [24–27]. Also, the lensing potential bi-spectrum and other higher-order statistics from the nonlinear growth of the LSS are detectable in the near future CMB experiments [25, 28–30].

The delensing using mass-tracers (such as galaxies and CIB) or reconstructed CMB lensing map could be also affected by the nonlinear growth of the LSS. The matter density fluctuations at late time of the universe are highly non-Gaussian. If mass tracers are used, the delensed B mode by such non-Gaussian fields can have additional contributions from the higher-order correlations between the density fluctuations and lensing potential. As a result, the power spectrum of the delensed B mode is modified. In addition, the covariance of the delensed B-mode spectrum is also affected by the non-Gaussianity of the density fluctuations at low redshifts. If the reconstructed lensing potential is used for delensing, the statistics of the delensed B mode becomes more complicated. For example, the power spectrum of the delensed B-mode contains, at least, four- and six-point correlations of CMB anisotropies and has higher-order correlations of the lensing potential.

This paper addresses the impact of the nonlinear growth of the LSS on B-mode delensing by simulations. We compute full-sky maps of galaxy distributions and lensed CMB maps based on N-body simulations. The CMB deflection angle published by Ref. [31] is also used for making the lensed CMB maps. The delensing is performed by computing the template of the lensing B mode and subtracting it from the "observed" B mode. We then compute the statistics of the delensed B mode such as the angular power spectrum and its correlation coefficients.

This paper is organized as follows. Section II recalls the basic methodology of the delensing. Section III briefly describes our simulations used in our analysis. Section IV presents our main results. Section V sum-

marizes our work. In addition to the nonlinear growth effect on delensing, appendix A shows the survey boundary and sky projection effects in delensing.

Throughout this paper, we adopt the flat ΛCDM (lambda cold dark matter) model consistent with the WMAP 9-yr result [32]. The cosmological parameters are the matter density $\Omega_{\rm m} = 0.279$, the baryon density $\Omega_{\rm b} = 0.046$, the cosmological constant $\Omega_\Lambda = 0.721$, the Hubble parameter $h = 0.7$, the amplitude of density fluctuations $\sigma_8 = 0.82$, and the spectral index $n_{\rm s} = 0.97$.

II. DELENSING

Here we briefly summarize notations in this paper and methods of the delensing.

A. Lensed CMB anisotropies

The lensing effect on the CMB anisotropies is well described by a remapping of the primary CMB anisotropies (e.g. [33]). Denoting the primary CMB temperature and polarization anisotropies as $\Theta(\hat{\boldsymbol{n}})$ and $Q(\hat{\boldsymbol{n}}) \pm \mathrm{i}U(\hat{\boldsymbol{n}})$, the lensed CMB anisotropies in a direction $\hat{\boldsymbol{n}}$ are obtained by

$$\widetilde{\Theta}(\hat{\boldsymbol{n}}) = \Theta(\hat{\boldsymbol{n}} + \boldsymbol{d}(\hat{\boldsymbol{n}})) , \qquad (1)$$

$$[\widetilde{Q} \pm \mathrm{i}\widetilde{U}](\hat{\boldsymbol{n}}) = [Q \pm \mathrm{i}U](\hat{\boldsymbol{n}} + \boldsymbol{d}(\hat{\boldsymbol{n}})) . \qquad (2)$$

Here, $\boldsymbol{d}(\hat{\boldsymbol{n}})$ is the deflection angle, and is usually decomposed into the gradient and curl modes, $\boldsymbol{\nabla}\phi$ and $(\star\boldsymbol{\nabla})\varpi$ [8], but the curl mode is negligible in the standard ΛCDM simulation [31, 34].

The harmonic coefficients of the scalar quantities, Θ and ϕ, are obtained by the (spin-0) spherical harmonics transform, while the polarization parameters, Q and U, are transformed to the following E and B modes by the spin-2 spherical harmonics, $_{\pm 2}Y_{\ell m}$:

$$[E \pm \mathrm{i}B]_{\ell m} = -\int \mathrm{d}\hat{\boldsymbol{n}} \,_{\pm 2}Y^*_{\ell m}(\hat{\boldsymbol{n}})[Q \pm \mathrm{i}U](\hat{\boldsymbol{n}}) . \qquad (3)$$

Expanding Eq. (2) up to the first order of the lensing potential, the lensing-induced B-mode is given by (e.g. [35])

$$B^{\rm lens}_{\ell m} = -\mathrm{i} \sum_{\ell' m'} \sum_{LM} \begin{pmatrix} \ell & \ell' & L \\ m & m' & M \end{pmatrix} \mathcal{S}_{\ell \ell' L} E_{\ell' m'} \phi_{LM} , \quad (4)$$

where ϕ_{LM} is the harmonic coefficients of the lensing potential, and we ignore the primary B mode and lensing curl mode. The quantity $\mathcal{S}_{\ell \ell' L}$ represents the mode coupling induced by lensing:

$$\mathcal{S}_{\ell \ell' L} = \sqrt{\frac{(2\ell+1)(2\ell'+1)(2L+1)}{16\pi}} \begin{pmatrix} \ell & \ell' & L \\ 2 & -2 & 0 \end{pmatrix}$$
$$\times [-\ell(\ell+1) + \ell'(\ell'+1) + L(L+1)] . \quad (5)$$

Here, the above quantity is unity if $\ell + \ell' + L$ is an odd integer and zero otherwise.

B. Delensing

A method to remove lensing contributions in observed B modes is to make a template of the lensing B modes (hereafter, lensing template) with a measured CMB lensing map and E mode [7, 11]. The lensing template up to first order of the CMB lensing potential is defined as [17–19, 36]

$$B^{\rm res}_{\ell m} = -\mathrm{i} \sum_{\ell' m'} \sum_{LM} \begin{pmatrix} \ell & \ell' & L \\ m & m' & M \end{pmatrix} \mathcal{S}_{\ell \ell' L} W^E_{\ell'} \widehat{E}_{\ell' m'} W^x_L \widehat{x}_{LM} , \tag{6}$$

where $\widehat{E}_{\ell' m'}$ is the observed E mode, $\widehat{x}_{LM} = x_{LM} + n_{LM}$ is an observed mass tracer which correlates with the CMB lensing potential. In this paper, $\widehat{x}$ is either the galaxy density fields or reconstructed CMB lensing potential. The quantity W^E_ℓ is the E-mode Wiener filter defined as $W^E_\ell = C^{\rm EE}_\ell / \widehat{C}^{\rm EE}_\ell$, where $C^{\rm EE}_\ell$ and $\widehat{C}^{\rm EE}_\ell$ denote the angular power spectra of E and $\widehat{E}$, respectively. Similarly, the filter for the galaxy density map or CMB lensing potential is given by $W^x_L = C^{\phi x}_L / \widehat{C}^{xx}_L$ where $\widehat{C}^{xx}$ is the observed power spectrum of the measured mass tracer fields. In the galaxy delensing, the observed galaxy power spectrum contains the shot noise in the measurement of the galaxy number density. In the CMB lensing potential, the observed power spectrum is computed as the sum of the lensing potential spectrum and Gaussian reconstruction noise.

In computing the lensing template from the galaxy density map, we use the galaxy density fields and E modes up to $\ell = 2048$. For the CMB internal delensing, we reconstruct the lensing potential using $\Theta\Theta$ or EB quadratic estimator [37, 38]. The CMB multipoles between $\ell = 500$ and 2048 are used for the reconstruction without the CMB instrumental noise.

III. SIMULATION

Here, we describe our method of the N-body and ray-tracing simulations and how to simulate the lensed CMB maps and galaxy distribution.

We first provide a short summary of the N-body and ray-tracing simulations. For detailed description, we refer readers to our previous paper [31]. We performed cosmological N-body simulations of dark matter to reproduce the inhomogeneous mass distribution in the universe, which naturally includes the non-Gaussian fluctuations. Here, we followed the gravitational evolution of 2048^3 particles in cubic simulation boxes by using a public code Gadget2 [39, 40]. The cubic boxes have side lengths of $450, 900, 1350, \ldots, 6300\,h^{-1}$Mpc from low to high redshift ($z \leq 7.1$). We chose an arbitrary point in the box as the observer's position and constructed spherical lens shells with a thickness of $150 h^{-1}$ Mpc around the observer (which locates at the center of shells). Median radius of the i-th shell is $150 \times (i + 1/2)\,h^{-1}$Mpc
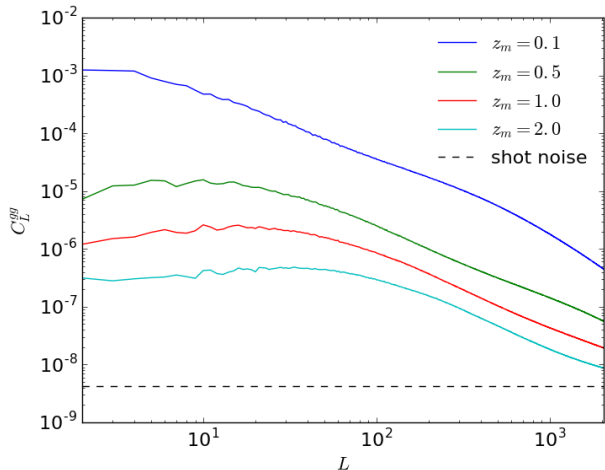
FIG. 1. The galaxy power spectrum with varying the mean redshift of galaxies, $z_{\rm m} = 0.1$, 0.5 1.0 and 2.0. The power spectrum is obtained from the simulations with the nonlinear growth.

($i = 0, 1, 2, \dots$) in comoving scale. The inner shell is taken from the smaller box at lower redshift. Then, we projected N-body particles onto each lens shell, and calculated surface mass density and deflection angle. For higher redshifts ($z = 7.1 - 1100$), we prepared the lens shells based on the Gaussian fluctuations (instead of N-body method), which is a good approximation in the linear regime. Light rays, emitted from the observer, are deflected at each lens shell, and these ray paths are numerically evaluated up to the last scattering surface. Therefore, the simulation includes the post-Born correction. We used a public code `GRayTrix`[1] [41, 42] for this ray-tracing computation. This code also calculate the convergence, shear and rotation. The code relies on the `Healpix` scheme [43], and we adopt the angular resolution of $N_{\rm side} = 4096$ throughout this paper. Then, we numerically obtained the deflection angle $\boldsymbol{d}(\hat{\boldsymbol{n}})$ on the full sky maps. We prepared 104 such maps in total. We checked that the power spectra of lensing potential agree with the theoretical prediction calculated by `CAMB` [44] within 5% up to $\ell = 3000$ (see Section 3.5 of Ref. [31]).

The lensed CMB maps are generated as follows. We first create unlensed Gaussian CMB maps which do not contain primary B modes, using the CMB temperature and E-mode angular power spectra computed by `CAMB`. Then, we use the above CMB deflection angles to remap the unlensed CMB temperature and polarization maps. We do not include the CMB instrumental noise in the lensed CMB maps.

Using the above N-body simulation, we also generate 104 full-sky maps of the galaxies distribution. We pop-

ulate "galaxies" as biased tracers of density contrast on the lens shells, based on given bias parameter $b(z)$ and radial number density distribution $dn/dz(z)$. We assume a simple scale-independent bias, $b(z) = \sqrt{1 + z}$ [45]. The number density of galaxies is 20 [arcmin^{-2}]. The normalized galaxy redshift distribution is assumed to be (e.g. [46])

$$N(z) = \frac{\beta}{z_0 \Gamma[(1+\alpha)/\beta]} \left(\frac{z}{z_0}\right)^{\alpha} \exp\left[-\left(\frac{z}{z_0}\right)^{\beta}\right], \quad (7)$$

where the parameter, z_0, is determined by the mean redshift of the galaxies, $z_{\rm m}$:

$$z_0 = z_{\rm m} \frac{\Gamma[(1+\alpha)/\beta]}{\Gamma[(2+\alpha)/\beta]}. \quad (8)$$

We choose $\alpha = 2$ and $\beta = 1$. We vary the mean redshift, z_m, from 0.1 to 2.0. The galaxy distribution with $z_m = 1$ mimics a galaxy sample in the ongoig Subaru Hyper Suprime-Cam survey [47].

In addition to the above maps, we also generate random Gaussian fields of galaxy distribution and lensing potential whose power spectra coincide with that obtained from the simulations with the nonlinear growth. The lensing potential is generated so that the correlation between the lensing potential and galaxy distribution coincides with that of the simulation with the nonlinear growth. Then, the lensed CMB maps produced by using the Gaussian lensing potential are generated.

Fig. 1 shows the angular power spectrum of the galaxy distribution at each redshift measured from the simulation with the nonlinear growth, compared with the shot noise spectrum. The measured power spectra are dominated by the signal. Fig. 2 shows the correlation coefficients of the angular power spectrum, i.e.,

$$R_{bb'} = \frac{{\rm Cov}_{bb'}}{\sqrt{{\rm Cov}_{bb}{\rm Cov}_{b'b'}}}, \quad (9)$$

where ${\rm Cov}_b$ is the covariance of the binned angular spectrum defined as

$$\mathrm{Cov}_{bb'} = \langle C_b^{gg} C_{b'}^{gg}\rangle - \langle C_b^{gg}\rangle\langle C_{b'}^{gg}\rangle, \quad (10)$$

and $\langle\cdots\rangle$ denotes the average over 104 realizations of our simulation. The correlation coefficients become significant at lower redshifts because the nonlinear growth of LSS leads to a non-Gaussianity in the density fluctuations. At large scales ($L \lesssim 100$), the nonlinear growth in the galaxy distribution decreases and the off-diagonal elements become zero. Even at $z_{\rm m} = 1$, the correlation becomes ~ 0.3 at $L_1 \sim L_2 \gtrsim 1000$. The galaxy distribution at $z_{\rm m} \lesssim 1$ is highly non-Gaussian.

On the other hand, Fig. 3 shows the correlation coefficients of the CMB lensing potential power spectrum. The correlation coefficients of the lensing power spectrum are not significant as the gravitational potential at high redshift, $z \sim 2$, is the dominant source of the CMB lensing effect.
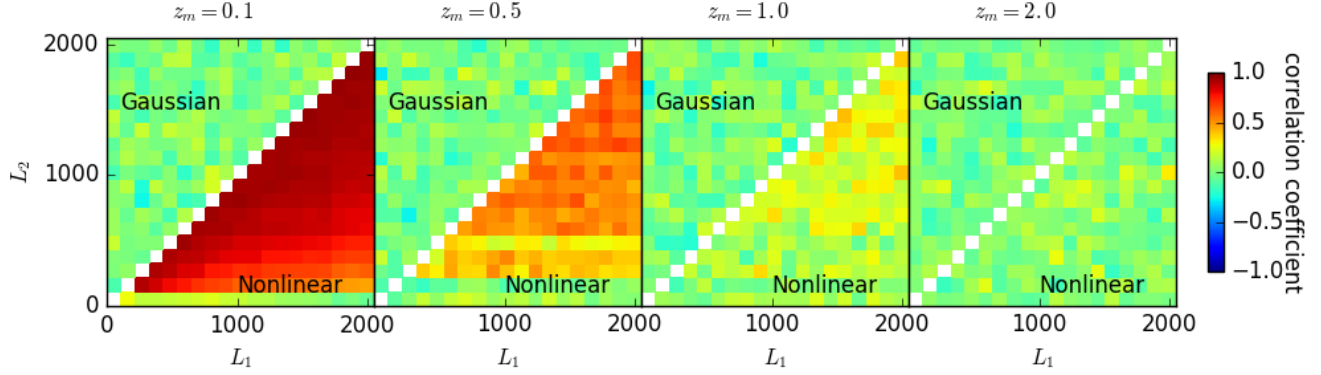
FIG. 2. The correlation coefficients of the galaxy power spectrum with varying the mean redshift of galaxies, $z_{\rm m} = 0.1$, 0.5 1.0 and 2.0. We show the cases with the random Gaussian simulation (upper left) or the simulation with the nonlinear growth (lower right).
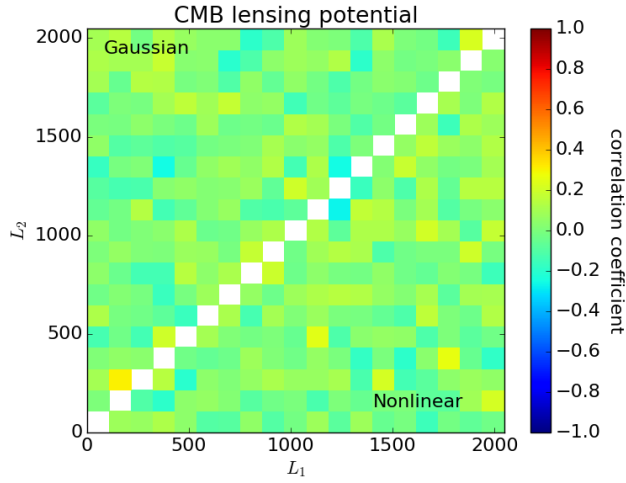

FIG. 3. The correlation coefficients of the CMB lensing potential power spectrum.

FIG. 4. Fractional difference of the lensing or delensed B-mode spectra between the Gaussian and nonlinear-growth simulations. The delensing of B mode is performed using a simulated galaxy distribution with the mean redshift of $z_{\rm m} = 0.5$ or 2.0, or a reconstructed CMB lensing map from $\Theta\Theta$ / EB quadratic estimator.

IV. RESULTS

The difference of the delensing results between the Gaussian and nonlinear-growth simulations appear in the angular power spectrum and its covariance. The discrepancy in the delensed B-mode spectrum leads to a bias in the estimate of the primary B mode contributions. The increase of the covariance degrades the delensing efficiency and signal-to-noise ratio of the primary B modes. In the following sections, we summarize the discrepancy of the results between the Gaussian and nonlinear simulations.
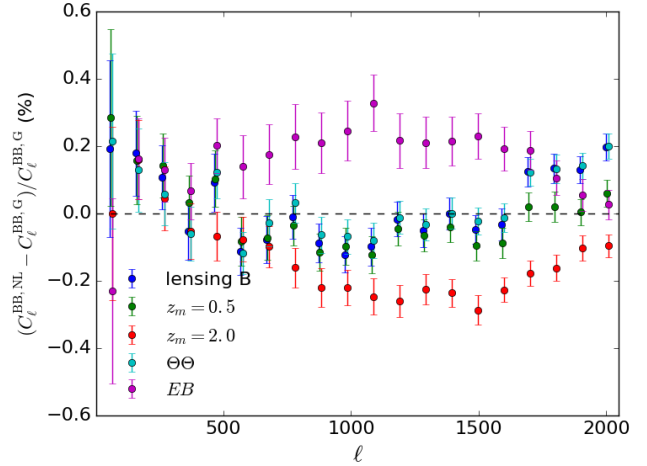
A. Delensed B-mode power spectrum

Fig. 4 shows the fractional difference of the lensing or delensed B-mode power spectra between the Gaussian and nonlinear-growth simulations. As shown in Fig. 1 of Ref. [48], the nonlinear growth of the LSS produces additional sub-percent contributions in the lensing B-mode power spectrum. Our result is consistent with Ref. [48].

The nonlinear growth also leads to additional contributions in the delensed B-mode spectra. The fractional change to the delensed B-mode spectrum with a mass tracer of $z_{\rm m} = 0.5$ or $\Theta\Theta$ quadratic estimator is similar
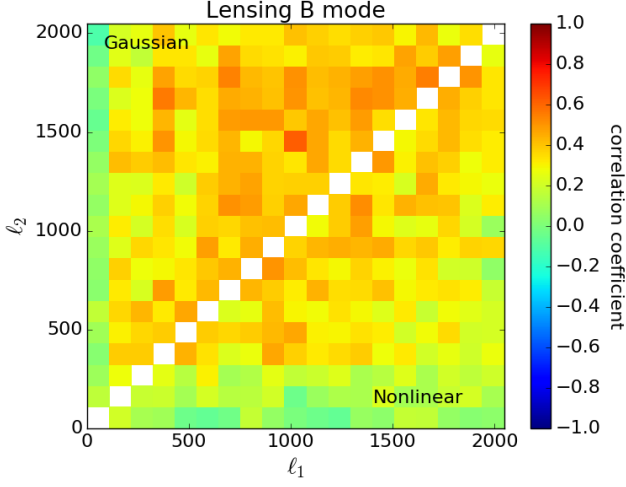
FIG. 5. The correlation coefficients of the lensing B-mode power spectrum.

to that to the lensing B mode. This is because the delensing efficiency is not so high (see Fig. 8 below), and the nonlinear contributions in the delensed B mode is not significantly different from that in the lensing B mode. On the other hand, if we use the galaxies with $z_\mathrm{m} = 2.0$, the fractional difference becomes sub-percent and is more significant than that in the case with $z_\mathrm{m} = 0.5$ or the $\Theta\Theta$ estimator. This indicates that the nonlinear structure is not effectively removed even if the delensing efficiency is improved. Finally, if we use the reconstructed lensing map from the EB estimator, the fractional difference becomes positive. Since the delensing efficiency using the EB estimator is much better than that in the other cases, other nonlinear terms would remain in the fractional difference. In addition, the bias comes from the correlation between the B modes to be delensed and in the EB estimator [12, 50]). This correlation is approximately proportional to the lensing B mode, and leads to the additional nonlinear contribution in the fractional difference. As described above, while the behavior of the nonlinear contribution in the B-mode spectra depends on the mass tracer, the nonlinear contribution in the lensing/delensed BB spectrum is not significant compared to the statistical error expected in the ongoing and near future CMB experiments.

B. Correlation coefficients of power spectrum

Fig. 5 shows the correlation coefficients of the lensing B-mode spectrum (the B-mode spectrum without delensing). As shown in [49], the non-Gaussianity becomes significant at smaller scales. Our results show that the nonlinear growth effect does not significantly change the correlations.

Fig. 6 shows the correlation coefficients of the delensed

B-mode power spectrum, and the difference of the coefficients between the delensed and lensing B-mode spectra. In all cases, the nonlinear growth does not significantly affect the correlation coefficients of the delensed B-mode spectrum.

We also check that the change of the variance of the lensing/delensed B-mode spectrum by the inclusion of the nonlinear growth is also not significant.

To see how the non-Gaussianity of the galaxy distribution shown in Fig. 2 is suppressed, Fig. 7 shows the off-diagonal covariance of the lensing template given by Eq. (6). As indicated by Fig. 2, the lensing template with mass tracers at low z is also a non-Gaussian field and has non-negligible correlation coefficients of the power spectrum. This large correlation coefficients seen for low-z templates make them sub-optimal estimators for the lensing B-modes shown in Fig. 6. Even using low-z mass tracers, however, the delensed B-mode spectrum is not significantly affected by the nonlinear growth. This is partly because the off-diagonal correlation matrix of the lensing template contributes to that of the delensed B mode after scaled by, $\sqrt{f_b f_{b'}}$, with $f_b \equiv C_b^{\mathrm{BB,temp}}/C_b^{\mathrm{BB,res}}$ [2]. As shown in Fig. 8, the delensing efficiency decreases by decreasing the redshift of the mass tracers. For low-z tracers, the scaling factor therefore becomes $f_b = (C_b^{\mathrm{BB}} - C_b^{\mathrm{BB,res}})/C_b^{\mathrm{BB,res}} \ll 1$.

Fig. 9 shows the correlation coefficients of the delensed B-mode spectrum using the CMB derived lensing potential reconstructed using the $\Theta\Theta$ or EB quadratic estimators. Similar to the galaxy delensing case, the impact of the nonlinear growth is not significant. We check that the change of the variance of the delensed B-mode spectrum by the inclusion of the nonlinear growth is also not significant. Note that, while the impact of the nonlinear growth is not important, the simulation results indicate that the off-diagonal element of the covariance using EB estimator has non-trivial non-Gaussian feature at smaller scales. One possibility of the origin of this feature is that the B mode to be delensed correlates with the B mode in the lensing reconstruction (see e.g. [50]). The detailed study on the covariance of the delensed B mode using EB estimator is highly involved, and will be investigated in our future work.

----

[2] The correlation coefficients of the delensed B-mode spectrum is given by $R_{bb'}^{\mathrm{res}} \simeq (\langle C_b^{\mathrm{BB,res}} C_{b'}^{\mathrm{BB,res}}\rangle - C_b^{\mathrm{BB,res}} C_{b'}^{\mathrm{BB,res}})/2\sqrt{C_b^{\mathrm{BB,res}} C_{b'}^{\mathrm{BB,res}}}$. This contains the correlation coefficients of the lensing template spectrum as $R_{bb'}^{\mathrm{res}} \supset (\langle C_b^{\mathrm{BB,temp}} C_{b'}^{\mathrm{BB,temp}}\rangle - C_b^{\mathrm{BB,temp}} C_{b'}^{\mathrm{BB,temp}})/2\sqrt{C_b^{\mathrm{BB,res}} C_{b'}^{\mathrm{BB,res}}} \simeq R_{bb'}^{\mathrm{temp}} \sqrt{f_b f_{b'}}$ with $f_b = C_b^{\mathrm{BB,temp}}/C_b^{\mathrm{BB,res}}$.
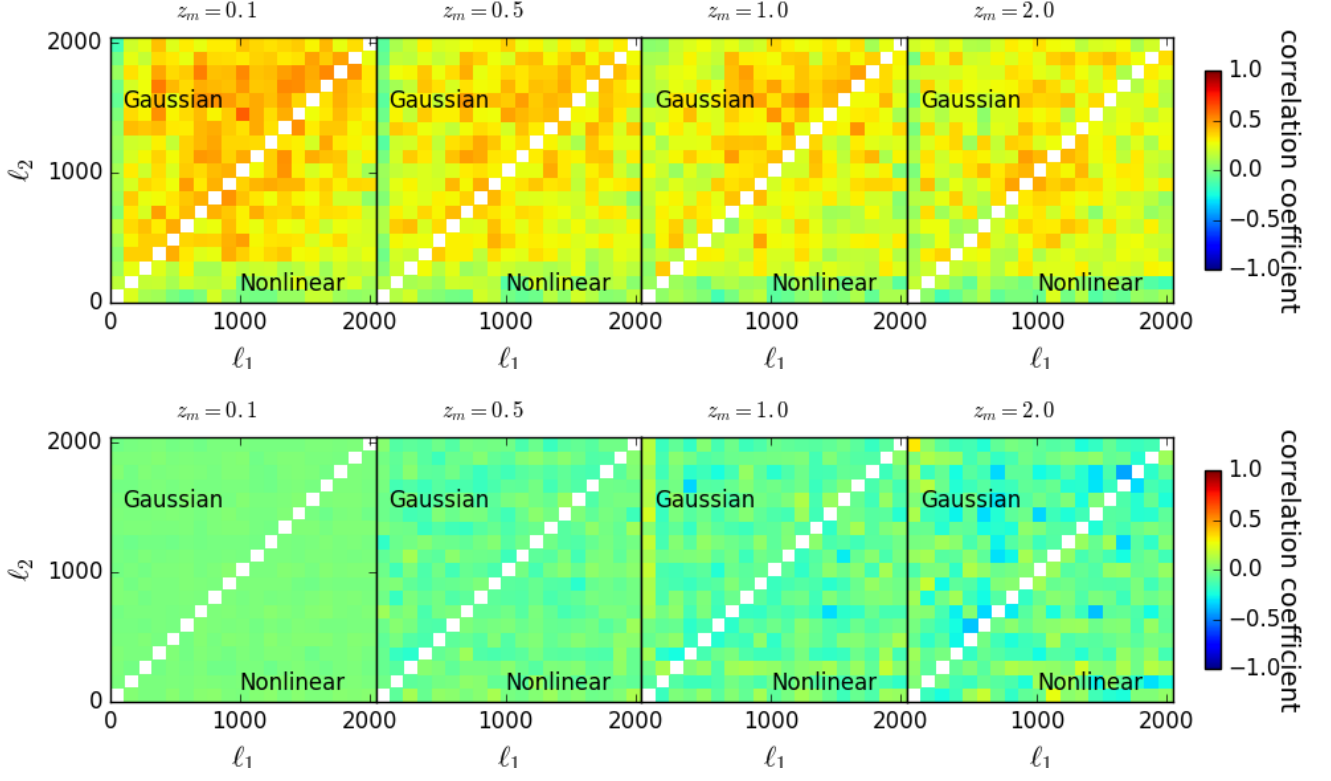
FIG. 6. **Top**: The correlation coefficients of the delensed B-mode power spectrum using galaxy distribution at $z_m = 0.1$, $z_m = 0.5$, $z_m = 1.0$ and $z_m = 2.0$ from left to right. **Bottom**: The difference of the correlation coefficients between the delensed and lensing B-mode spectrum.
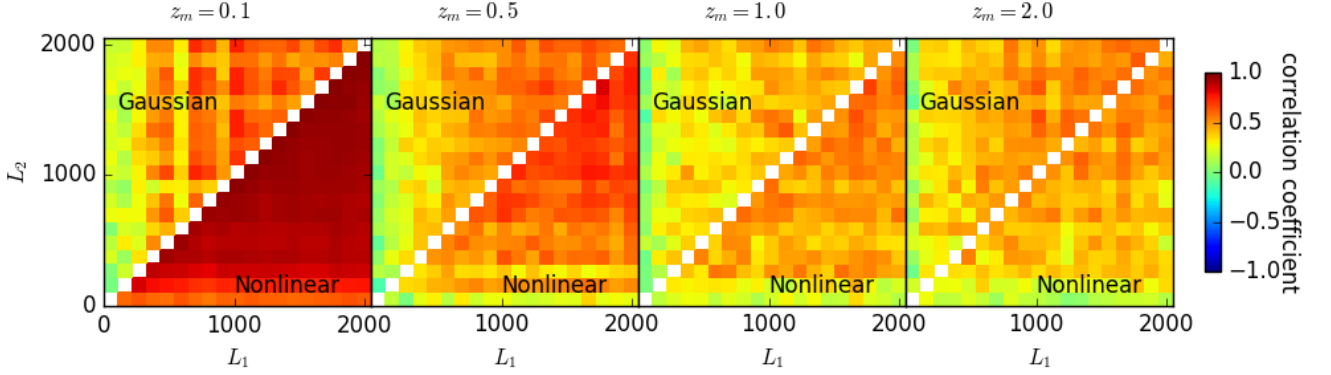

FIG. 7. The correlation coefficients of the lensing template spectrum using galaxy distribution at $z_m = 0.1$, 0.5, 1.0 and 2.0.

C. Power spectrum amplitude

To quantify the impact of the nonlinear growth on the delensed B-mode spectrum, we evaluate the statistical error of the amplitude of the angular power spectrum (i.e. the inverse of the signal-to-noise of the power spectrum).

The amplitude is estimated from (e.g., [51, 52])

$$A = \frac{1}{\sum_b w_b} \sum_b w_b \frac{\widehat{C}_b}{C_b^{\mathrm{ref}}}, \qquad (11)$$

with $w_b = \sum_{b'} C_b^{\mathrm{ref}} \mathrm{Cov}_{bb'}^{-1} C_{b'}^{\mathrm{ref}}$. If the off-diagonal elements of the correlation coefficients are significant, the statistical error of the above amplitude increases.
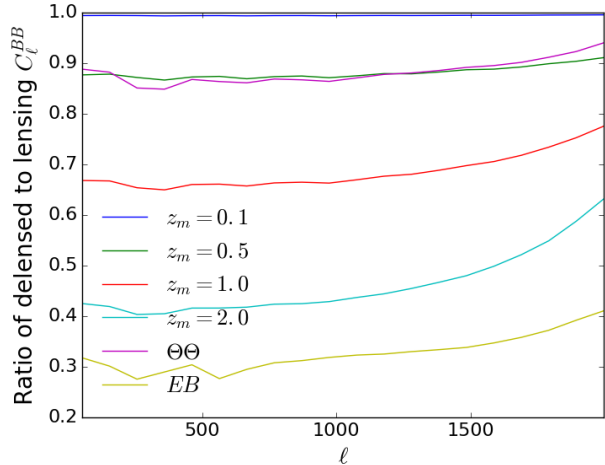
FIG. 8. Ratio of the delensed to lensing B-mode power spectrum with varying the mean redshift of the galaxy survey. We also show the ratio with $\Theta\Theta/EB$ quadratic estimator. The simulation with the nonlinear growth is used.

TABLE I. The variance of the power spectrum amplitude, $\sigma(A) \times 10^3$, using 104 realizations of CMB/galaxy maps, with 20 multipole bins between $2 \leq L \leq 2048$.

	Gauss	Nonlinear
Lensing BB	1.89	1.91
$z_m = 0.1$	1.89	1.92
$z_m = 0.5$	1.82	1.78
$z_m = 1.0$	1.86	1.60
$z_m = 2.0$	1.40	1.55
$\Theta\Theta$	1.48	1.55
EB	1.86	1.92

Table I shows the variance of the power spectrum amplitude from 104 realizations. The covariance and C_b^{ref} are computed from the simulation. Even in the Gaussian cases, the off-diagonal elements of the correlation coefficients exist due to the non-Gaussianity of the lensing B mode. The variance decreases as the source redshift increases. This indicates that the delensing removes lensing contributions instead of adding additional nonlinear growth effects, and the off-diagonal covariance is suppressed. Within the simulation error, there are no significant difference between the results from the Gaussian and nonlinear growth simulations.

V. SUMMARY AND DISCUSSION

We explored the impact of the nonlinear growth of the LSS on delensing. We considered delensing using the galaxy distribution or the CMB-derived lensing potential. We found that the corrections to the delensed B-mode

spectrum are $\sim 0.3\%$ at $\ell = 1000 - 2000$ with high-z mass tracers ($z_{\mathrm{m}} \sim 2$). While the effect of the nonlinear growth is significant on the lensing template with low-z mass tracers, the correlation coefficients of the delensed B-mode spectrum are not significantly affected by the nonlinear growth. The impact of the nonlinear growth is also not significant on the correlation coefficients of the delensed B-mode spectrum with the CMB-derived lensing potential.

We ignored the CMB instrumental noise in the simulation. If the CMB noise is nearly Gaussian, the contribution from the noise does not create non-Gaussianity in the delensed B mode and our conclusion above is unchanged.

We focused on the galaxy distribution as a mass-tracer for delensing. The CIB is another interesting observable for the CMB delensing [17, 18]. The conclusion would be, however, also the same even if we use other mass tracers such as CIB because the signal part of mass tracers comes from the same underlying density fields. For example, in the CIB case, the source mostly comes from the density fluctuations at higher redshifts ($z \gtrsim 1$) (e.g. [53]), and the results would be similar to the case with $z_{\mathrm{m}} \sim 1 - 2$ in our simulation.

The lensed CMB maps, foreground matter distribution and a Fortran code to make mock galaxy distribution are publicly available. If you want to download them, please visit our website (http://cosmo.phys.hirosaki-u.ac.jp/takahasi/allsky_raytracing/).

Appendix A: Delensing analysis for cut-sky

The main motivation of this paper is to see the impact of the nonlinear growth in the delensing analysis. However, in practical analysis, many other possible effects should be simultaneously taken into account. One
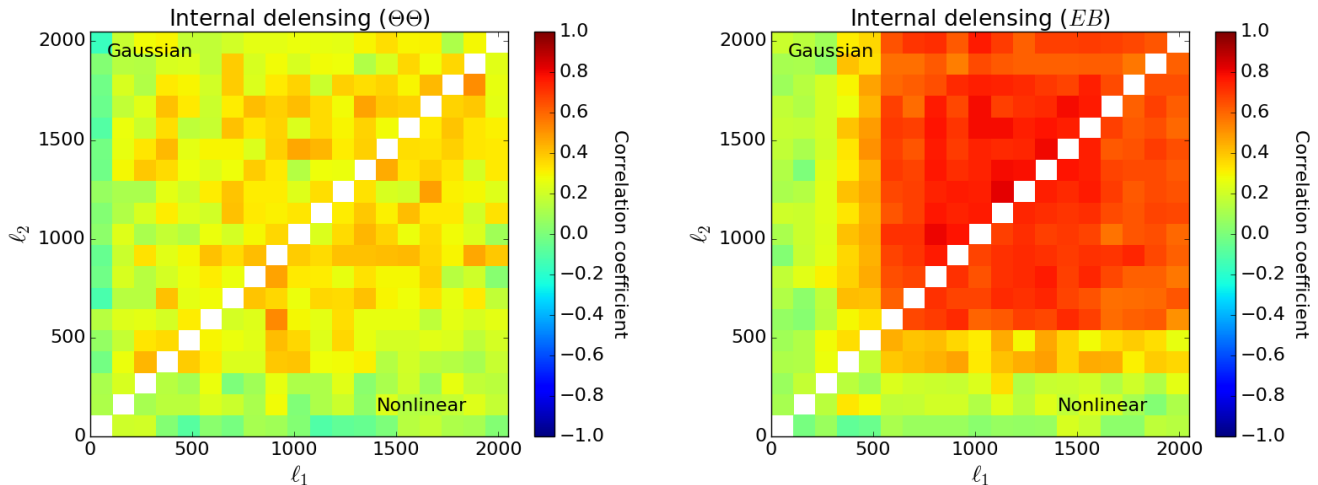
FIG. 9. The correlation coefficients of the delensed B-mode spectrum with CMB derived lensing potential using $\Theta\Theta$ (Left) or EB (Right) quadratic estimator.

of the most significant effects in the delensing analysis would be the survey boundary due to finite sky coverage and Galactic/point-source masking. In this section, we show some results of delensing using finite size of CMB and galaxy density maps.

1. Analysis in cut-sky

Since the difference of the results between the Gaussian and nonlinear simulations is very small, we only use the nonlinear-growth simulation in the cut-sky analysis. We cut 5×5 deg^2 region from each realization of the lensed CMB map and galaxy density map at $z_{\mathrm{m}} = 1$. The size of this patch is chosen to mimic the overlap region between the Subaru-Hyper Suprime Cam [54] and Polarbear [55, 56]. These maps are then multiplied by a simple analytic apodization function and transformed to Fourier space. For the lensed CMB maps, we reduce E-to-B leakage by applying the χ-field estimator [57]. The delensing in flat sky is performed by first constructing the lensing template from the cut-sky E mode and galaxy density, and then removing it from the observed B mode. We simply apply the full-sky diagonal Wiener filter for E mode and galaxy density fields in constructing the lensing template in flat sky. This simplification could make the delensing process sub optimal, but this approach is computationally easy for the implementation. The multipole range of the E mode and galaxy density fields is the same as that in the full-sky analysis. We ignore the CMB instrumental noise.
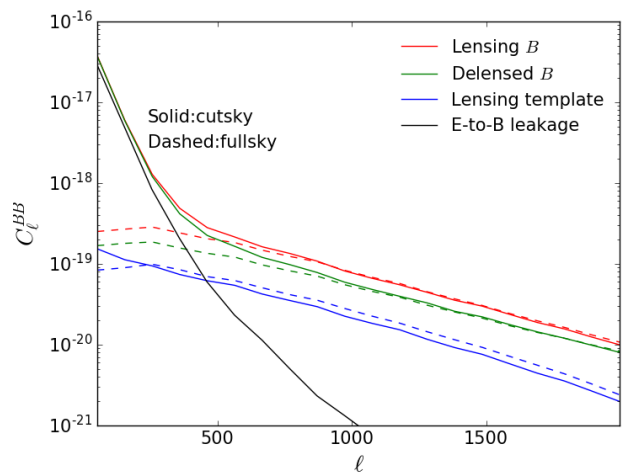

FIG. 10. The lensing and delensed B-mode spectrum from the 5×5 deg^2 cut-sky map. The delensing uses the galaxy number density with $z_{\mathrm{m}} = 1$.

2. Delensed B-mode spectrum and its correlation coefficient

Fig. 10 shows the lensing and delensed B-mode spectra in cut-sky analysis, compared with those obtained from the full-sky analysis. The E-to-B leakage is obtained by removing the B mode before the map is cut. At large scale ($\ell < 500$), the B-mode spectrum is dominated by the leakage from the E mode due to the survey boundary and sky projection effect. The lensing template in cut-sky is slightly suppressed compared to that in full-sky.

Fig. 11 shows the delensing efficiency, i.e., the ratio of the delensed (or E-to-B leakage) to lensing B-mode
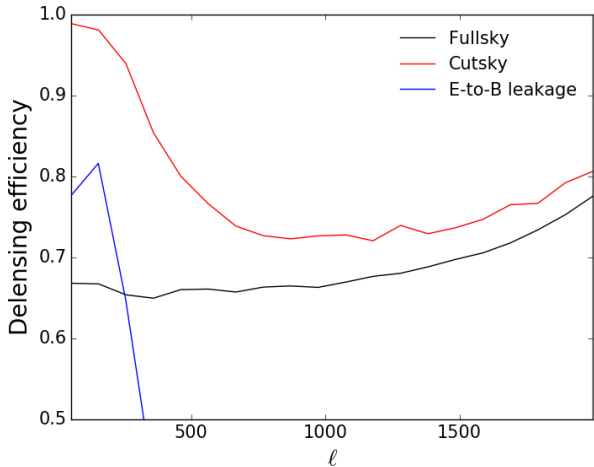
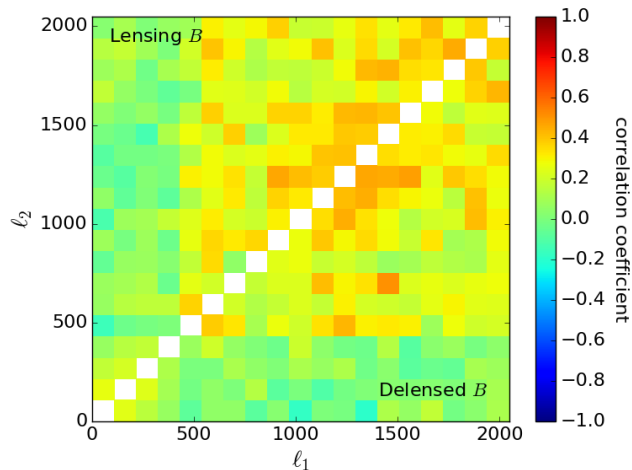FIG. 11. The delensing efficiency for the delensing using the cut-sky map.

FIG. 12. The correlation coefficients of the lensing and delensed B-mode spectrum from the cut-sky map.

spectrum. In cut-sky analysis, the delensing efficiency reduces by $\sim 5\%$ at small scales ($\ell \geq 1000$). At large scales ($\ell < 500$), the E-to-B leakage dominates the B mode, and this contribution should be removed in addition to the lensing B mode. One possible approach is to

use the matrix method as discussed in the BICEP/Keck Array analysis [58]. Even if the matrix method is applied, the large-scale B mode measurement from ground suffers from e.g. the 1/f noise, and the delensing of the B mode at $\ell < 500$ is relatively not important for the Polarbear-like patch considered here.

Fig. 12 shows the correlation coefficient of the B-mode spectrum in cut-sky. As shown in Fig. 6, in full sky, the delensing procedure reduces the correlation coefficients of
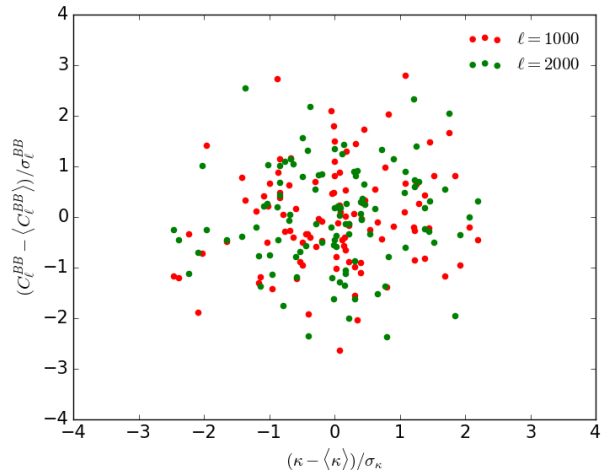

FIG. 13. Correlation between the mean convergence and lensing B-mode spectrum at the 5×5 deg^2 patch. The operation, $\langle \cdots \rangle$, is the average over the simulation realizations.

the delensed B-mode spectrum. In contrast, the correlation coefficients are almost not decreased by the removal of the lensing B mode in cut-sky.

Finally, in Fig. 13, we show the correlation between the mean convergence in the small patch and the lensing B-mode power spectrum to see the effect of the super-survey mode [59]. If the super-survey mode is significant, the power spectrum highly correlates with the mean convergence. We find that the correlation coefficient is at percent level and the super-survey mode is negligible. The analytic estimate of this effect is studied by Ref. [60], and the impact of the super-survey mode is shown to be negligible in the lensing B mode spectrum. Our result is consistent with their results and justifies the approximation in their paper.

[1] M. Kamionkowski and E. D. Kovetz, *"The Quest for B Modes from Inflationary Gravitational Waves"*, Ann. Rev. Astron. Astrophys. **54** (2016) 227–269, [arXiv:1510.06042].

[2] J. A. Grayson and others (BICEP3 Collaboration), *"BICEP3 performance overview and planned Keck Array upgrade"*, Proc. SPIE Int. Soc. Opt. Eng. **9914** (2016) 99140S, [arXiv:1607.04668].

[3] Simons Observatory Collaboration, *"The Simons Observatory: Science goals and forecasts"*, arXiv:1808.07445.

[4] BICEP2 Collaboration, *"BICEP2/Keck Array IV:*

Optical Characterization and Performance of the BICEP2 and Keck Array Experiments", Astrophys. J. **806** (2015) 206.

[5] L. Knox and Y.-S. Song, *"A Limit on the detectability of the energy scale of inflation"*, Phys. Rev. Lett. **89** (2002) 011303, [astro-ph/0202286].

[6] M. Kesden, A. Cooray, and M. Kamionkowski, *"Separation of gravitational wave and cosmic shear contributions to cosmic microwave background polarization"*, Phys. Rev. Lett. **89** (2002) 011304, [astro-ph/0202434].

[7] U. Seljak and C. M. Hirata, *"Gravitational lensing as a contaminant of the gravity wave signal in CMB"*, Phys. Rev. D **69** (2004) 043005, [astro-ph/0310163].

[8] C. M. Hirata and U. Seljak, *"Reconstruction of lensing from the cosmic microwave background polarization"*, Phys. Rev. D **68** (2003) 083002, [astro-ph/0306354].

[9] Z. Pan, E. Anderes, and L. Knox, *"Approximate Likelihood Approaches for Detecting the Influence of Primordial Gravitational Waves in Cosmic Microwave Background Polarization"*, Phys. Rev. D **97** (2018) 103512, [arXiv:1709.00102].

[10] M. Millea, E. Anderes, and B. D. Wandelt, *"Bayesian delensing of CMB temperature and polarization"*, arXiv:1708.06753.

[11] K. M. Smith *et al.*, *"Delensing CMB Polarization with External Datasets"*, J. Cosmol. Astropart. Phys. **06** (2012) 014, [arXiv:1010.0048].

[12] W.-H. Teng, C.-L. Kuo, and J.-H. P. Wu, *"Cosmic Microwave Background Delensing Revisited: Residual Biases and a Simple Fix"*, arXiv:1102.5729.

[13] N. Sehgal, M. S. Madhavacheril, B. Sherwin, and A. van Engelen, *"Internal Delensing of Cosmic Microwave Background Acoustic Peaks"*, arXiv:1612.03898.

[14] D. Green, J. Meyers, and A. van Engelen, *"CMB delensing beyond the B modes"*, arXiv:1609.08143.

[15] A. Challinor *et al.*, *"Exploring cosmic origins with CORE: Gravitational lensing of the CMB"*, J. Cosmol. Astropart. Phys. **2018** (2018) 018, [arXiv:1707.02259].

[16] J. Carron, *"Optimal constraints on primordial gravitational waves from the lensed CMB"*, arXiv:1808.10349.

[17] G. Simard, D. Hanson, and G. Holder, *"Prospects for Delensing the Cosmic Microwave Background for Studying Inflation"*, Astrophys. J. **807** (2015) 166, [arXiv:1410.0691].

[18] B. D. Sherwin and M. Schmittfull, *"Delensing the CMB with the Cosmic Infrared Background"*, Phys. Rev. D **92** (2015) 043005, [arXiv:1502.05356].

[19] T. Namikawa, D. Yamauchi, D. Sherwin, and R. Nagata, *"Delensing Cosmic Microwave Background B-modes with the Square Kilometre Array Radio Continuum Survey"*, Phys. Rev. D **93** (2016) 043527, [arXiv:1511.04653].

[20] P. Larsen, A. Challinor, B. D. Sherwin, and D. Mak, *"Demonstration of Cosmic Microwave Background Delensing Using Cosmic Infrared Background"*, Phys. Rev. Lett. **117** (2016) 151102, [arXiv:1607.05733].

[21] SPTpol Collaboration (Manzotti, A. et al.), *"CMB polarization B-mode delensing with SPTPol and Herschel"*, Astrophys. J. **846** (2017) 1, [arXiv:1701.04396].

[22] J. Carron, A. Lewis, and A. Challinor, *"Internal delensing of Planck CMB temperature and polarization"*, J. Cosmol. Astropart. Phys. **05** (2017) 035, [arXiv:1701.01712].

[23] *Planck* Collaboration, *"Planck 2018 results. VIII. Gravitational lensing"*, arXiv:1807.06210.

[24] V. Boehm, M. Schmittfull, and B. Sherwin Phys. Rev. D **94** (2016) 043519, [arXiv:1605.01392].

[25] G. Pratten and A. Lewis, *"Impact of Post-Born lensing on the CMB"*, J. Cosmol. Astropart. Phys. **08** (2016) 047, [arXiv:1605.05662].

[26] V. Boehm, B. D. Sherwin, J. Liu, J. C. Hill, M. Schmittfull, and T. Namikawa, *"On the effect of non-Gaussian lensing deflections on CMB lensing measurements"*, arXiv:1806.01157.

[27] D. Beck, G. Fabbian, and J. Errard, *"Lensing Reconstruction in Post-Born Cosmic Microwave Background Weak Lensing"*, arXiv:1806.01216.

[28] T. Namikawa, *"CMB Lensing Bispectrum from Nonlinear Growth of the Large Scale Structure"*, Phys. Rev. D **93** (2016) 121301, [arXiv:1604.08578].

[29] J. Liu, J. C. Hill, B. Sherwin, A. Petri, V. Boehm, and H. Zoltan, *"CMB lensing beyond the power spectrum: Cosmological constraints from the one-point probability distribution function and peak counts"*, Phys. Rev. D **94** (2016) 103501, [arXiv:1608.03169].

[30] T. Namikawa, F. R. Bouchet, and A. Taruya, *"The CMB lensing bi-spectrum as a probe of modified gravity theories"*, arXiv:1805.10567.

[31] R. Takahashi *et al.*, *"Full-sky Gravitational Lensing Simulation for Large-area Galaxy Surveys and Cosmic Microwave Background Experiments"*, Astrophys. J. **850** (2017) 24, [arXiv:1707.01472].

[32] G. Hinshaw *et al.* (WMAP Collaboration) Astrophys. J. **208** (2013) 19, [arXiv:1212.5226].

[33] A. Lewis and A. Challinor, *"Weak gravitational lensing of the CMB"*, Phys. Rep. **429** (2006) 1–65, [astro-ph/0601594].

[34] S. Saga, D. Yamauchi, and K. Ichiki, *"Weak lensing induced by second-order vector mode"*, Phys. Rev. D **92** (2015) 063533.

[35] W. Hu, *"Weak lensing of the CMB: A harmonic approach"*, Phys. Rev. D **62** (2000) 043007, [astro-ph/0001303].

[36] A. Manzotti, *"Future cosmic microwave background delensing with galaxy surveys"*, Phys. Rev. D **97** (2018) 043527, [arXiv:1710.11038].

[37] W. Hu and T. Okamoto, *"Mass Reconstruction with CMB Polarization"*, Astrophys. J. **574** (2002) 566–574, [astro-ph/0111606].

[38] T. Okamoto and W. Hu, *"The angular trispectra of CMB temperature and polarization"*, Phys. Rev. D **66** (2002) 063008, [astro-ph/0206155].

[39] V. Springel, N. Yoshida, and S. D. M. White, *"GADGET: a code for collisionless and gasdynamical cosmological simulations"*, New Astronomy **6** (2001) 79–117, [astro-ph/0003162].

[40] V. Springel, *"The cosmological simulation code GADGET-2"*, Mon. Not. R. Astron. Soc. **364** (2005) 1105–1134, [astro-ph/0505010].

[41] T. Hamana, J. Sakurai, M. Koike, and L. Miller, *"Cosmological constraints from Subaru weak lensing cluster counts"*, Publ. Astron. Soc. Jpn. **67** (2015) 34, [arXiv:1503.01851].

[42] M. Shirasaki, T. Hamana, and N. Yoshida, *"Probing cosmology with weak lensing selected clusters - I. Halo*

approach and all-sky simulations", Mon. Not. R. Astron. Soc. **453** (2015) 3043–3067, [arXiv:1504.05672].

[43] K. Gorski *et al.*, *"HEALPix - A Framework for high resolution discretization, and fast analysis of data distributed on the sphere", Astrophys. J.* **622** (2005) 759–771, [astro-ph/0409513].

[44] A. Lewis, A. Challinor, and A. Lasenby, *"Efficient Computation of CMB anisotropies in closed FRW models", Astrophys. J.* **538** (2000) 473–476, [astro-ph/9911177].

[45] A. Rassat *et al.*, *"Deconstructing Baryon Acoustic Oscillations: A Comparison of Methods"*, arXiv:0810.0003.

[46] T. Namikawa, S. Saito, and A. Taruya, *"Probing dark energy and neutrino mass from upcoming lensing experiments of CMB and galaxies", J. Cosmol. Astropart. Phys.* **1012** (2010) 027, [arXiv:1009.3204].

[47] H. Aihara *et al.*, *"The Hyper Suprime-Cam SSP Survey: Overview and survey design", Publ. Astron. Soc. Jpn.* **70** (Jan., 2018) S4, [arXiv:1704.05858].

[48] A. Lewis and G. Pratten, *"Effect of lensing non-Gaussianity on the CMB power spectra", J. Cosmol. Astropart. Phys.* **12** (2016) 003, [arXiv:1608.01263].

[49] A. Benoit-Levy, K. M. Smith, and W. Hu, *"Non-Gaussian structure of the lensed CMB power spectra covariance matrix", Phys. Rev. D* **86** (2012) 123008, [arXiv:1205.0474].

[50] T. Namikawa, *"CMB internal delensing with general optimal estimator for higher-order correlations", Phys. Rev. D* **95** (2017) 103514, [arXiv:1703.00169].

[51] BICEP2 Collaboration and Keck Array Collaboration, *"BICEP2/Keck Array VIII: Measurement of Gravitational Lensing from Large-scale B-mode Polarization", Astrophys. J.* **833** (Dec., 2016) 228,

[arXiv:1606.01968].

[52] BICEP2 Collaboration and Keck Array Collaboration, *"BICEP2 / Keck Array IX: New bounds on anisotropies of CMB polarization rotation and implications for axionlike particles and primordial magnetic fields", Phys. Rev. D* **96** (Nov., 2017) 102003, [arXiv:1705.02523].

[53] *Planck* Collaboration, *"Planck 2013 results. XXX. Cosmic infrared background measurements and implications for star formation", Astron. Astrophys.* (2014) A30.

[54] Subaru Hyper Suprime-Cam Collaboration, *"Hyper Suprime-Cam Design Review Booklet"*, . http://anela.mtk.nao.ac.jp/hypersuprime/presentation/hscreview20090227final_combined.pdf.

[55] POLARBEAR Collaboration (Z. D. Kermish et al.), *"The POLARBEAR experiment", Proc. SPIE* **8452** (2012) 84521C.

[56] POLARBEAR Collaboration (T. Tomaru et al.), *"The POLARBEAR-2 experiment", Proc. SPIE* **8452** (2012) 84521H.

[57] K. M. Smith, *"Pseudo-c(l) estimators which do not mix E and B modes", Phys. Rev. D* **74** (2006) 083002, [astro-ph/0511629].

[58] Bicep2 / *Keck Array* Collaboration, *"BICEP2 / Keck Array VII: Matrix Based E/B Seperation Applied to* Bicep2 *and the Keck Array", Astrophys. J.* **825** (2016) 66, [arXiv:1603.05976].

[59] M. Takada and W. Hu, *"Power spectrum super-sample covariance", Phys. Rev. D* **87** (June, 2013) 123504, [arXiv:1302.6994].

[60] A. Manzotti, W. Hu, and A. Benoit-Levy, *"Super-Sample CMB Lensing", Phys. Rev. D* **90** (2014) 023003, [arXiv:1401.7992].